7-1-2011

Electronic properties of metal-arene functionalized graphene

Pavel Plachinda
Portland State University

David Evans
Portland State University

Raj Solanki
Portland State University

Citation Details

Plachinda, P., Evans, D. R., & Solanki, R. (2011). Electronic properties of metal-arene functionalized graphene. Journal Of Chemical Physics, 135(4), 044103.

Electronic properties of metal-arene functionalized graphene

Paul Plachinda,[a] David R. Evans,[1,2] and Raj Solanki[1]
[1]*Department of Physics, Portland State University, 1719 SW 10th Avenue, Portland, Oregon 97207-0751, USA*
[2]*Sharp Laboratories of America, Inc., 5750 Northwest Pacific Rim Boulevard, Camas, Washington 98607-9489, USA*

(Received 26 April 2011; accepted 27 June 2011; published online 22 July 2011)

We have employed first-principles density-functional calculations to study the electronic characteristics of covalently functionalized graphene by metal-bis-arene chemistry. It is shown that functionalization with M-bis-arene (M = Ti, V, Cr, Mn, Fe) molecules leads to an opening in the bandgap of graphene (up to 0.81 eV for the Cr derivative), and as a result, transforms it from a semimetal to a semiconductor. The bandgap induced by attachment of a metal atom topped by a benzene ring is attributed to modification of π-conjugation and depends on the concentration of functionalizing molecules. This approach offers a means of tailoring the band structure of graphene and potentially its applications for future electronic devices. © *2011 American Institute of Physics*. [doi:10.1063/1.3613649]

I. INTRODUCTION

Graphene continues to draw immense interest because of its unusual electronic and spin properties resulting from a simple structure composed of a single layer of carbon atoms arranged in a two-dimensional honey-comb pattern.[1] These properties, including ballistic carrier transport and quantum Hall effect, make it a promising candidate as a building block of future nanoelectronic devices and as a possible replacement for silicon.[2] In spite of graphene's amazing properties, there are some obstacles that need to be overcome before it can be considered as a viable candidate to replace silicon. The main barrier is absence of a bandgap. Therefore, producing a bandgap is probably one of the most important challenges that must be addressed before graphene can ultimately enable practical applications ranging from digital electronics to infrared nanophotonics.

A number of possible solutions have been proposed and demonstrated for producing bandgaps in single- and double-layered graphene. One of the more straightforward methods involves growth of epitaxial graphene on a lattice matched (SiC) substrate to induce a stress and, as a result, open up a bandgap of about 0.26 eV.[3] Alternatively, a somewhat more successful method utilizes quantum confinement to open a bandgap in graphene by fabrication of nanoscale structures, i.e., quantum dots and nanoribbons, where the bandgap varies inversely with the nanoscale structure dimension.[4] However, the non-uniform edges of these structures play a major role in degrading their electrical properties.[5] For example, with graphene nanoribbon of widths less than 10 nm, a bandgap of about 0.4 eV has been reported; however, associated electron motilities are between 100–200 cm^2 /V s. Mobility is believed to be degraded by edge scattering[6]

A graphene bilayer shares many of the interesting properties of a single-layered film and provides a richer band structure, albeit without a bandgap. Theoretical studies have predicted that a significant bandgap could be induced by breaking the inversion of the two layers through the application of a perpendicular electric field.[7] Using a single or double (top and bottom) gates to apply a strong electric field, tunable bandgap of up to about 250 meV has been created in graphene FETs.[8,9]

Chemical modification of graphene by covalently functionalizing its surface potentially allows a wider flexibility in engineering electronic structure, in particular, the local density of states of the carbon atoms bound to the modifier that can result in opening of the bandgap. Such binding can involve covalent hydrogenation of graphene to modify hybridization of carbon atoms from sp^2 to sp^3 geometry[10,11] (see Fig. 1(a)). Methods have also been developed to functionalize graphene covalently with molecular species.[12–14] Among these, perfluorophenylazide (PFPA) functionalization of graphene is well developed using a nitrene intermediate (see Fig. 1(c)). We have utilized films of this molecule to act as adhesion layers to produce long ribbons of exfoliated graphene.[13,14]

In order to minimize the effects of edge scattering of carriers, wider strips of graphene would be required for fabrication of devices; however, these wider strips will be semimetallic. Therefore, our objective is to identify molecules, when covalently bonded to graphene, can break its conical band structure and open up an energy gap. To achieve this goal, we have examined electronic structure of metal-arene (MA) functionalized graphene and report below our results based on first-principles density-functional calculations of the bandgap functionalized graphene (MA–Gr). It is shown that the MA covalently binds at the π-conjugation of graphene and changes the electronic properties from metallic to semiconducting. We also show that the energy gap can be tuned by adjusting the number of bound MA adducts.

During our previous investigation of utilizing PFPA as an adhesion layer, it was determined that PFPA was covalently bonded to graphene.[14] Hence, we first simulated the

[a]Author to whom correspondence should be addressed. Electronic mail: plachind@pdx.edu. Telephone: +001 503 725 4248. Fax: +001 503 725 2815.

TABLE I. Bandgaps of PFPA-functionalized graphene.

Element	B	C	N	O	P	S	Cl	As
Gap (eV)	∼0[a]	0.11	0.24	0	0.22	∼0[a]	0	∼0[a]

[a]Nonzero values below 0.001 Ha (∼0.027 eV) cannot be calculated exactly and therefore set to approximate zero.

covalent binding energy and the resulting induced bandgap in graphene of PFPA and its derivatives. (For the calculation methods–see below.) Derivatives that were considered were obtained by substituting the nitrogen in the nitrene radical by the element listed in Table I. It can be seen that the widest gap of 0.24 eV can be induced in graphene is when it is functionalized with a single PFPA molecule per 6 × 6 graphene supercell. Functionalization with two molecules slightly increases the gap to 0.28 eV. This gap is not wide enough for fabrication of practical devices. Therefore, we next focused on MA-functionalized graphene.

II. METHODS

The calculations were conducted within the framework of the density functional theory (DFT) as implemented in the DMOL3 package.[17] The generalized gradient approximation (GGA) in BLYP (Ref. 18) exchange-correlation parameterization was used for both final geometry optimization and band structure calculation. Initial geometry optimization was performed using the local density approximation with the Vosko-Wilk-Nusair[19] correlation functional. A 6 × 6 graphene supercell with a vacuum space of 11.5 A normal to graphene plane was used. Geometry optimization convergence criterion was satisfied when the total energy change was less than of 3×10^{-5} Ha. Only one k-point (Gamma) was used throughout the calculations since the distance between neighboring k-points was only 0.077 1/A due to a large supercell choice. For the band structure computation, the k-path selected was Γ–M–K–Γ, with 24, 20, and 40 k-points on each segment correspondingly. Although the GGA approach systematically underestimates the bandgaps, we are primarily interested in the mechanism of gap opening. For that purpose, the GGA approach is expected to provide qualitatively correct information. A more precise GW approach is very costly on this system, consisting of a total of 94 atoms. The DMOL3 package utilizes numerical orbital basis set for the radial part of the wave function, centered on the atoms allowing including a thick vacuum layer without increase of the computation time.

To pursue the effect of adduct concentration on the electronic structures, we have considered two configurations by adding one or four MA molecules onto a 6 × 6 rhombus cell, respectively. The cell constitutes 72 carbon atoms of graphene and 1 metal, 6 carbon, and 6 hydrogen atoms of each MA molecule.

III. RESULTS AND DISCUSSION

Various studies conducted on adatoms of transition metals on graphene and carbon nanotubes have demonstrated broad potential for modifying the electronic structure of

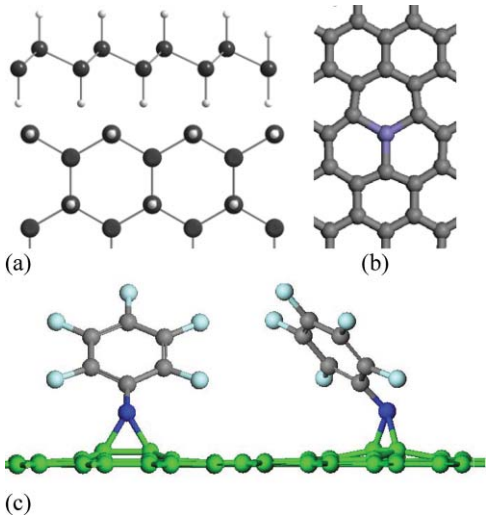

FIG. 1. View of the molecular structures of functionalized graphene. (a) Schematic drawing of hydrogenated graphene (Ref. 11) (carbon atoms are colored in black, hydrogen – white); (b) with metal adatom (Fe) (Ref. 15) (carbon atoms are colored in gray, metal – violet); (c) perperfluorophenylazide (PFPA) functionalized graphene (Ref. 16). (Carbon, nitrogen, and fluorine atoms are colored in gray (green for graphene), cyan, and blue, respectively.)

graphene.[15,16,20] Partially filled *d*-shells can play the role of electron donors[21] disturbing the π-conjugated system and, thus, possibly opening a gap. However, it was found that a single transition element adatom produces an insignificant charge transfer of ∼0.01 electrons per carbon atom from the transition metal to the graphene sheet, and thus hardly changes the band structure.[22] Even so, "sandwich compounds" such as metallocenes and bis-arenes have long been known and of great interest in inorganic chemistry. Moreover, it is well known that ligand aromaticity is preserved in these compounds; therefore, replacing one of the aromatic ligands with a graphene sheet would seem as an attractive method for functionalization since

(1) metallocenes and metal-bis-arene compounds are known to be good electronic donors[23] and graphene shows the strongest interaction with electron-donor and acceptor molecules via molecular charge transfer,[24]
(2) the geometrical structure of η^6 compounds is similar to the honeycomb structure of graphene.

Based on these observations, we undertook a study of metal-arene functionalized graphene for the following 3*d*-metals: Ti, V, Cr, Mn, Fe (Zn and Cu have closed 3*d* shell and therefore are ignored) in two different configurations – one and four MA molecules per 6 × 6 graphene supercell (Fig. 2).

A. Binding energy

The MA produces very strong bonds with the graphene sheet. Binding energy of Cr–MA was found by extrapolating to 0 K of the binding energies obtained by the Hess law for different values of thermal occupancy smearing. Quite high value of this energy – 4.72 eV (455.41 kJ/mol), which is about 25 kJ/mol per electron, indicates strong bonding and presents a solid evidence for real existence of such compounds.

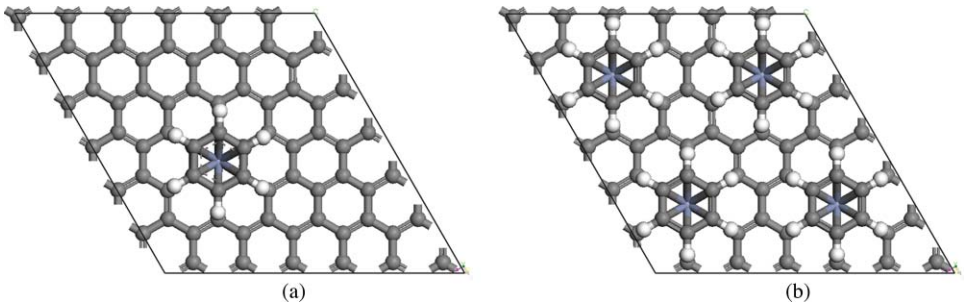

FIG. 2. Ball-and-stick presentation of optimized structures of MA-functionalized graphene (top view) with one (a) and four (b) MA adducts per 6 × 6 graphene supercell.

B. Possible synthesis strategy

The MA complexes are known to exist for all transition metals,[25] and their structure and chemistry resembles that of metallocenes. One of the many possible ways of synthesis is condensation of metal vapors on graphene, followed by aromatic molecules, such as benzene at low temperature and pressure. Elschenbroich and co-workers[26] have successfully applied this strategy to polyaromatics, which leads us to believe that this conventional synthesis approach may allow us to produce MA functionalized graphene sheets. By varying the concentration of metal vapor and aromatic molecules could provide a means to achieve different degree of functionalization.

C. Geometrical properties

We summarize in Table II the optimized configuration of MA-functionalized graphene.

As can be seen from Table II, the bonding to an "infinite" graphene sheet changes the structural features with respect to the free M[η^6-(arene)$_2$] molecule. General trends in the bonding lengths demonstrate following features: the M–C(graphene) bond lengths remain about 3% longer than the one in the free molecule; M–C(arene) bonds, however, remain almost unchanged with respect to the free molecules for Ti–Cr metals and become about 3% shorter for Mn and Fe. The reason for the extreme behavior of the bond lengths can be explained by considering a molecular orbital representation of the MAs. The usage of molecular orbitals (instead of Wannier functions as for a periodic system) is justified because we assume little interaction between the molecules from the neighboring cells. In the Cr[η^6-(arene)$_2$] electrons fully occupy a_{1g} binding orbital, whereas adding additional electrons, as happens in Mn and Fe leads to partial population of the anti-bonding, twice degenerate e_{1g}* orbital, which is composed of 4*p* and 4*s* atomic orbitals of the metal and anti-bonding π* orbitals of graphene and arene (see Table III).

The conjugated π-system of the graphene sheet can effectively redistribute additional electron density donated by the metal atom, and thus decrease the number of electrons on the M–C(graphene) bond, thus, weakening it. Deviation from the single molecule behavior for the M–C(arene) bond (Fig. 3(a)) is hardly observed for Ti, V, and Cr. In the case of Mn and Fe compounds, as mentioned above, demonstrate about 3% shortening of the bond. We relate this distortion to the Jahn-Teller effect: unpaired electrons in the Mn and Fe compounds occupy doubly degenerate e_{1g}* level and therefore, Mn and Fe compounds undergo geometrical distortion that removes degeneracy. This asymmetry in bond length also leads to the difference in C(arene)–M–C(graphene) angles: for Ti–Cr they exceed those for free molecule, but Mn–Fe are less. This phenomenon results in less mixing of the localized atomic *d*-orbitals and leads to creation of narrow bands in the band structure of MA–Gr, decreasing the bandgap compared to corresponding Ti–Cr compounds.

D. Electronic properties

The graphene-metal interaction in haptic functionalization has direct consequences for electronic properties of graphene. As previously reported, functionalization of graphene with radical (primarily hydrogen, epoxide, and nitrene) groups locally disrupt the planarity of the graphene sheet, changing local hybridization form sp^2 to sp^3 geometry,[10,11] which induces a sp^3-type defect-like state near the Fermi level. (Hereinafter under the Fermi level in insulators we understand the top of the valence band, where it is conventionally put by the majority of the DFT programs.) In

TABLE II. Geometrical parameters of free MA molecules and MA molecules bound to graphene sheet.

Metal atom	Ti	V	Cr	Mn	Fe
∠(C–M–C) (°) (MA)	103.477	101.397	99.76	101.285	104.353
M–C(a) (A)	2.312	2.255	2.211	2.244	2.314
∠(C–M–C) (°) (1-mol)	105.411	101.433	101.183	99.748	97.475
M–C(a)/M–C(g) (A)	2.361/2.368	2.295/2.310	2.235/2.266	2.171/2.266	2.186/2.358
∠(C–M–C) (°) (4-mol)	105.346	102.886	100.991	100.198	102.835
M–C(a) / M–C(g) (A)	2.335/2.391	2.26/2.334	2.216/2.274	2.161/2.298	2.198/2.394

TABLE III. Electronic configuration of the metal atoms in the MA, and the corresponding energy gap opening in the MA–Gr as the result of functionalization.

Metal atom	Ti	V	Cr	Mn	Fe
Number of valence electrons	16	17	18	19	20
Electronic configuration:					
e^*_{1g} (yz, xz)				↑	↑↑
a'_{1g} (z^2)		↑	↓↑	↓↑	↓↑
e_{2g} (x^2-y^2, xy)	↓↑↓↑	↓↑↓↑	↓↑↓↑	↓↑↓↑	↓↑↓↑
Number of unpaired electrons	0	1	0	1	2
Eg (1 molecule) (eV)	0.40815	0.10884	0.38094	0.29931	0
Eg (4 molecule) (eV)	0.32652	0.78909	0.8163	0	0.48978

our case, however, the graphene sheet is not distorted in the z-direction and thus re-hybridization of carbon atoms does not occur. The local bonding configuration is, however, significantly affected by the electronic structure of the functionalizing atom, and especially its d-electrons that were found to lie close to the Fermi level. This is similar to the situation with sp^3-type "impurity" states for the radical functionalization. Partially occupied highly localized d-orbitals near the Fermi level cause repulsion of the π-bands, causing the energy band of pristine graphene to be shifted away from the Fermi level due to the π-d interaction.

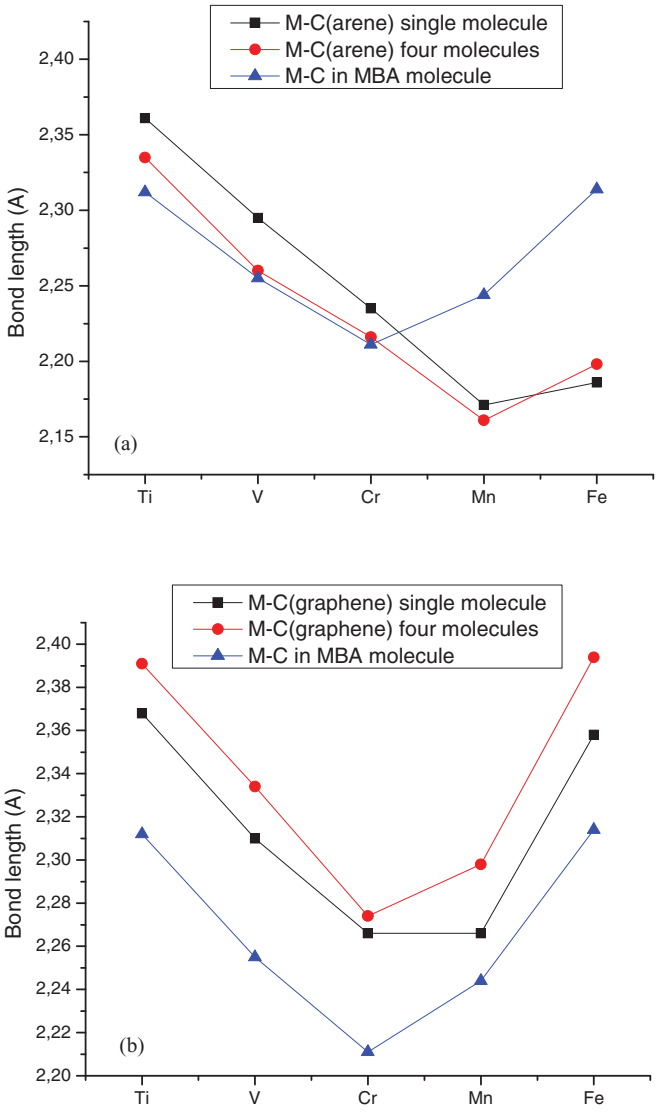

FIG. 3. Geometrical parameters of the MA–Gr (a) M–C(arene) bond length, (b) M–C(graphene) bond length.

The calculated band structures for CrBA-functionalized graphene are compared with pristine graphene in Fig. 4. It is readily observable that after haptic functionalization, the linear dispersion law of pristine graphene at the Dirac point is entirely broken. Since the calculations were conducted using 6 × 6 super cell, the K point maps to the Γ point, due to folding of the reciprocal space. The π- and π*-bands in the Γ direction in pristine graphene have a separation of about 11.26 eV. The bands that were previously intersecting at the Dirac point are now shifted together at the new Γ point of the supercell. The π and π*-bands preserve their arrangement in the functionalized graphene; however, the distance between them grows from about 1 eV in 1-MA–Gr to 1.25 eV in 4-MA–Gr. (This growth is attributed to the shift of the π* band by +0.25 eV relative to the 1-MA–Gr.) As the analysis of the density of states calculated for different atoms and projected on different angular momenta demonstrates, a system of pure (with no π-admixture) localized d-bands of the metal is now located between the π- and π*-bands of graphene, preventing them from crossing. These d-bands cause strong repulsion and are responsible for the opening of the gap now between the bands produced by the metal. These electronic properties of MA-functionalized products contrast from the sp^3 re-hybridization and loss of π-electrons found upon addition of acceptor chemical groups or metals in other functionalization schemes.[9,15,27] The fact that the bandgap strongly depends on the nature of the functionalizing metal atom confirms our idea about the importance of the number of d-electrons or the modification of the band structure. Both occupied and empty d-levels of the metal form flat bands close to the top of the valence band. These "impurity" states are probably responsible for bringing the strongest contribution to the band repulsion, more than the d-admixture of the former pure π- and π*-bands. Additional flat d-bands produced by the localized electrons of the metal atoms in the MA–Gr can be

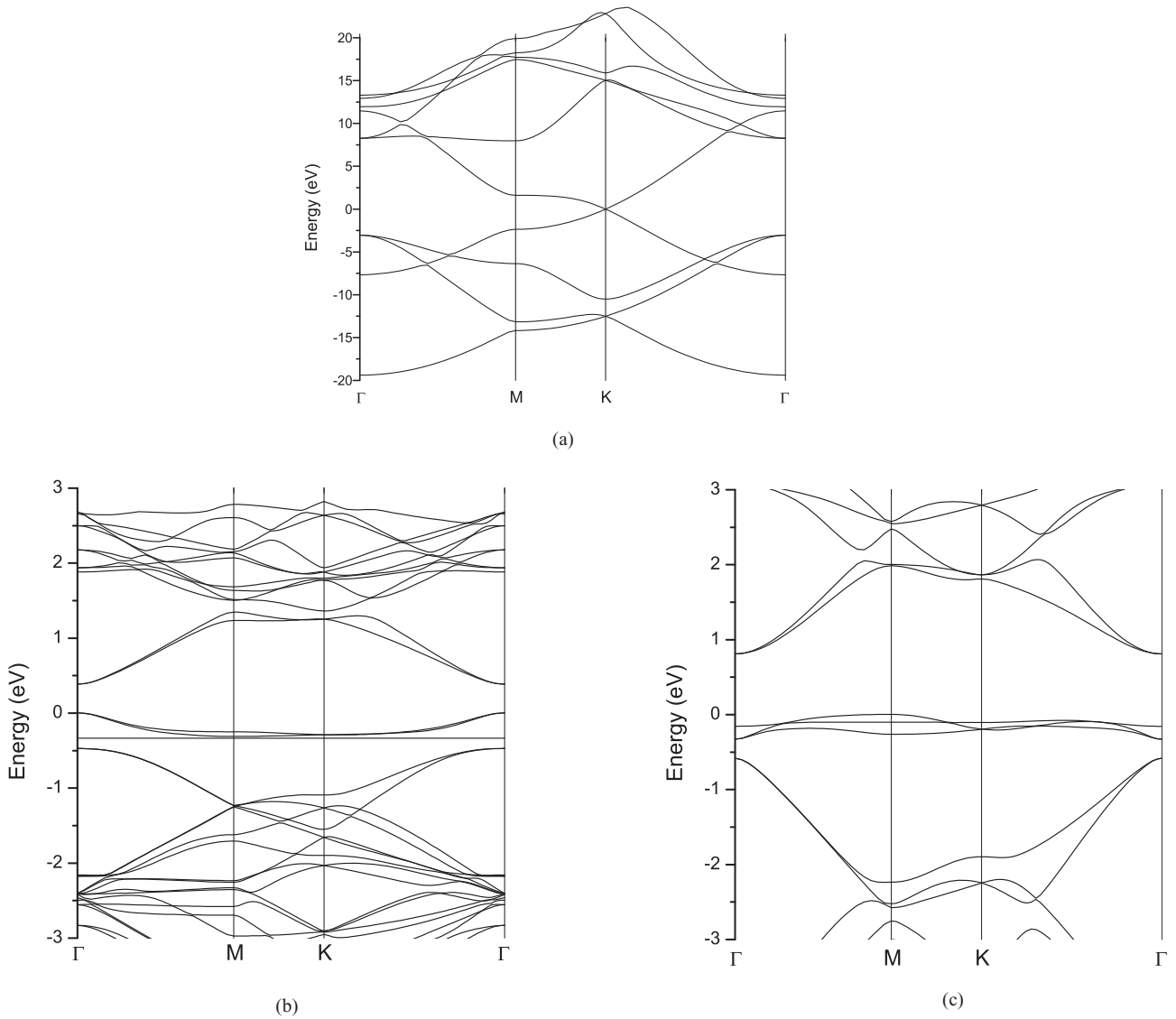

FIG. 4. Calculated band structures for pristine graphene (a), one single molecule CrBA functionalized graphene (b), and four molecules CrBA functionalized graphene (c).

successfully utilized to mimic dopant levels of conventional semiconductors.

An important property of the MA-induced perturbation of the band structure is that alteration in the electronic structure of graphene increases with increasing MA functionalization concentration. We have investigated the functionalization of graphene at higher adduct concentration by including three more MA functional groups in the unit cell (see Fig. 2). Due to the limitations imposed by the nature of the DFT calculations, we cannot study the variation of the electronic properties imposed by continuously changing concentration of functionalizing molecules. This would require dealing with huge supercells. Two aforementioned geometries correspond to one functionalizing molecule per 6×6 and 3×3 graphene supercells. An important idea is to demonstrate the ability to tweak the bandgap by varying the concentration, possibly even in the broader limits than discussed here. This corresponds to one MA molecule per 3×3 graphene supercell. Exact positions of functionalizing molecules inside the unit cell are not important since there are many ways to redefine the lattice. This geometry is further labeled as 4-MA–Gr unlike 1-MA–Gr with only one MA per 6×6 graphene supercell. As the concentration of functionalizing molecules increases (i.e., by transition from 1-MA–Gr to 4-MA–Gr) repulsion between the π-bands (graphene) increases as well, leading to the wider band opening. The extracted energy gap is 0.44 and 0.98 eV for one and four CrBA adducts (i.e., CrBA–Gr and 4-GrBA–Gr), respectively, on a graphene unit cell consisting of 72 graphene-carbon atoms. A higher number of *d*-bands complicates the picture. The distance between the π-bands in 1-VBA–Gr at the Γ-point is about 0.8 eV but "impurity" levels decrease it ten times to 0.08 eV. The distance between the *d*-levels in 1-MnBA–Gr is about 2.7 eV which is much more than the distance between π-bands, thus the highest occupied molecular orbital (HOMO) and the lowest unoccupied molecular level (LUMO) of 1-MnBA–Gr line up with the π and π^* bands of graphene. As the number of electrons in the system increases, the Fermi level drifts up causing a transition from a

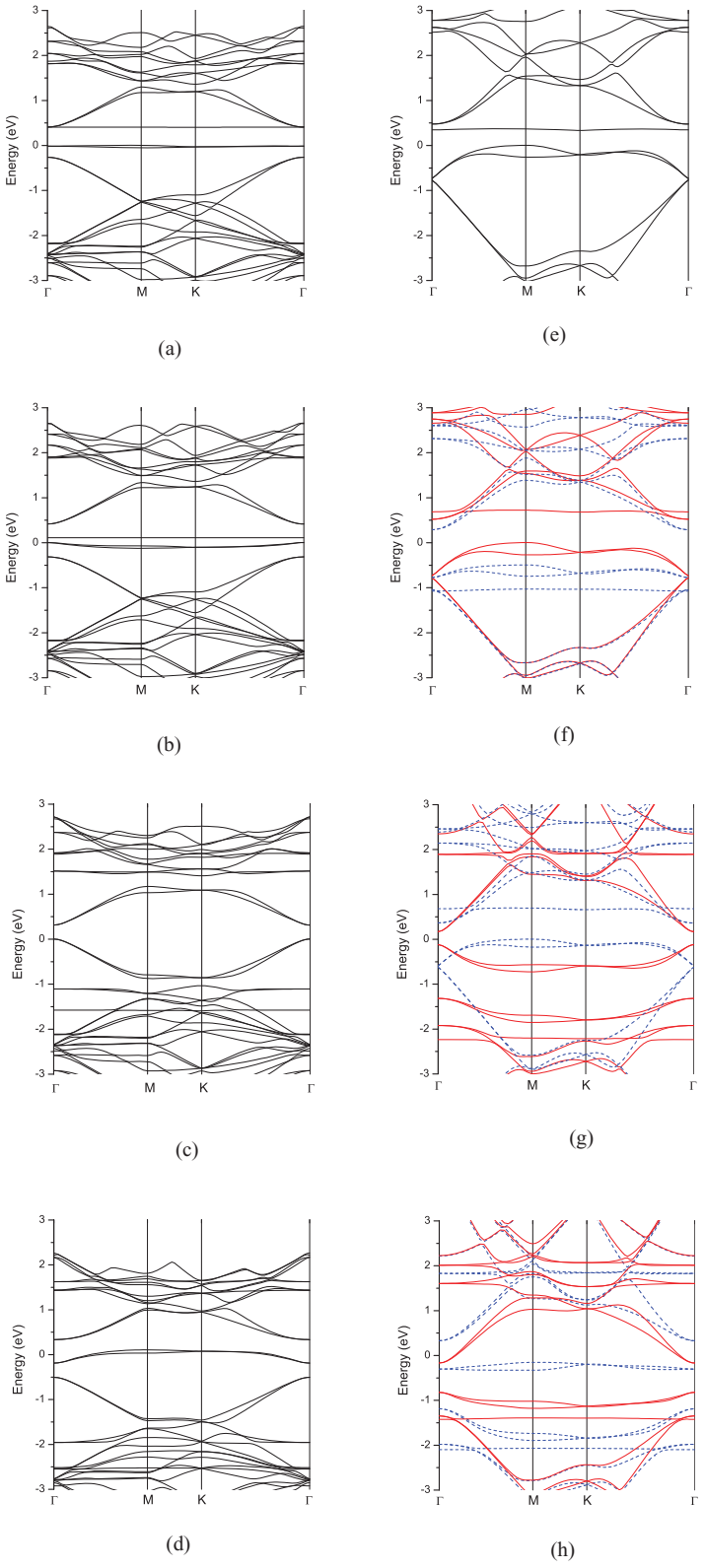

FIG. 5. Band structures of 1-MA–Gr (a–d) and 4-MA–Gr (e–h), where M = Ti, V, Mn, Fe. Red and blue coloring (solid and dashed lines in the offline version) correspond to spin-up and spin-down bands. Energy reference level coincides with the position of Fermi level

semiconductor to a metallic state. The band alignment of 1-MnBA–Gr and 1-FeBA–Gr is almost the same; however, due to the extra electron of Fe the Fermi level becomes coincident with the former π^*-band making the iron compound semimetallic. Same trend is observed in transition form 4-MnBA–Gr to 4-FeBA–Gr. The later becomes metallic for the very same reason: since the Fermi level is located higher in the iron compound, it becomes metallic even despite very close similarity of the band alignment between 4-MnBA–Gr and 4-FeBA–Gr. Band diagrams of all substances under consideration are presented in Fig. 5.

Closer analysis of band alignment demonstrates that gap opening can be primarily attributed to the interaction of the *d*-electrons with the π-conjugated system. Although the carbon atoms on graphene connecting to MA essentially retain a flat band configuration corresponding to sp^2 hybridization, additional π-*d* interaction is nevertheless present. Local modification of the original π-conjugation in the vicinity of the metal atom is manifested by re-hybridization, i.e., the HOMO and the LUMO of MA–Gr now are formed by the π-backbonding[28] mechanism. In some cases, however, this mechanism appears to be very weak, leaving *d*-orbitals of the metal atom almost unhybridized. This rehybridization, however, contrasts to conventional $sp^2 \rightarrow sp^3$ rehybridization because it occurs without major geometrical distortion of underlying graphene sheet. Accordingly, carrier scattering can be substantially regarded as due to electrostatic interaction similar to that observed for ionized dopant impurities in conventional semiconductors rather than due to localized defect states. As a consequence, it is to be expected that mobility degradation will be much less in MA–Gr than in covalently functionalized graphene for which significant non-planarity of the graphene sheet is unavoidable. Indeed, this is a crucial difference and was the original motivation for considering this type of functionalization, since it seems rather obvious that preservation of aromaticity vs sp^2 hybridization, should result in less degradation of carrier transport properties. Of course, this must be confirmed experimentally and work in that direction is in progress.

The charge densities of the corresponding HOMO/LUMO at the band center (the Γ point) are shown in Fig. 5. Different atoms demonstrate different mixing of atomic orbitals that take part in the formation of HOMO and LUMO. The HOMO of 1-CrBA–Gr and 1-MnBA–Gr (not shown) are constructed by the σ-type donation mechanism (empty *d*-orbital is interacting with filled π-orbital). The LUMO of these compounds and 1-VBA–Gr, in turn, demonstrate π-type back-donation behavior (filled *d*-orbital interacts with an empty π^*-orbital). The HOMO of 1-VBA–Gr is entirely represented by the d_z^2 orbital of the metal atom. The MO picture of 1-iron is somewhat different from the other atoms: π-type back-donation for HOMO and σ-type donation for LUMO. This is to be contrasted to 4-MA functionalization. As can be seen in Fig. 6, an increase of adduct concentration impedes the donation mechanism causing the HOMOs of 4-Cr, to consist of the unhybridized d_z^2 orbitals of the metal atom and the LUMO of the π-type back-donation MOs. Molecular orbitals of other MA–Gr structures are not shown here due to space limitations.

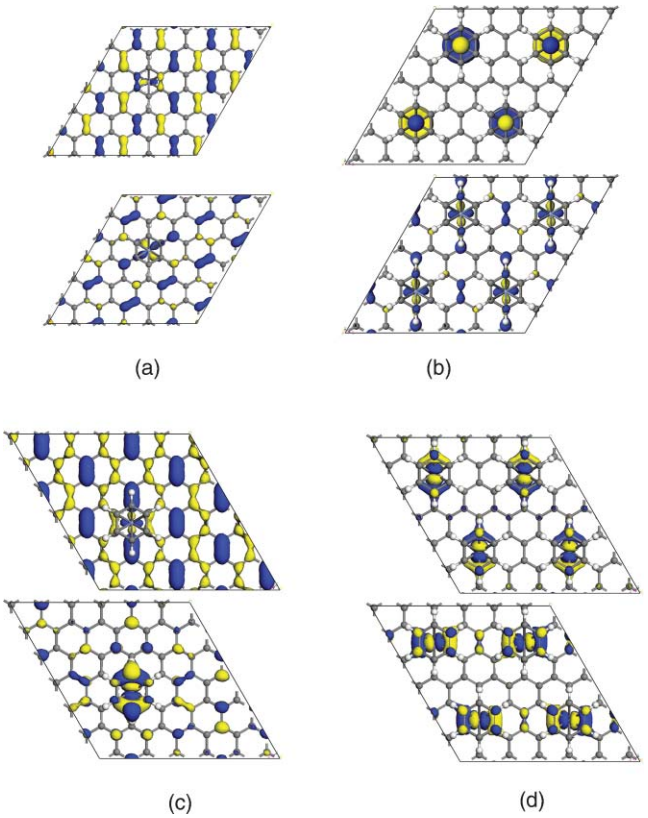

FIG. 6. Molecular orbitals (HOMO- top row, LUMO- bottom row) for 1-CrBA–Gr (a), 4-CrBA–Gr (b), 1-FeBA–Gr (c), 4-FeBA–Gr (d).

However, the donation mechanism changes depending on the number and energy of filled *d*-orbitals of the central atom. Proportional increase of functionalizing molecules causes a change of the amount of π-conjugated bonds broken due to the back-bonding mechanism. This correlates with the associated increase of the bandgap and thus provides support of the suggested scenario of the *d*-level-induced bandgap opening.

As it was previously demonstrated, graphene functionalized with transition metal atoms can demonstrate profound magnetic properties.[15] Band structures of 4-VBA–Gr and 4-FeBA–Gr (Figs. 7(a) and 7(b)) demonstrate strong spin polarization. Spin-unrestricted calculations reveal significant difference between spin-up (α) and spin-down (β) densities of states (DoS) pointing to ferromagnetic behavior of 4-VMB–Gr and 4-FeMB–Gr.

Iron demonstrates an even stronger difference in the DoS for the spin-up and spin-down electrons. Band structures for compounds with different central metal atoms having paired electrons obviously do not demonstrate any ferromagnetic behavior. However, due to presence of unpaired electrons, the manganese compound can exist in both ferromagnetic and antiferromagnetic states. A closer analysis of the magnetic properties of the MA–Gr will be published separately. The presence of nontrivial magnetic structure suggests wide possible applications of the MA functionalized graphene in spintronics.

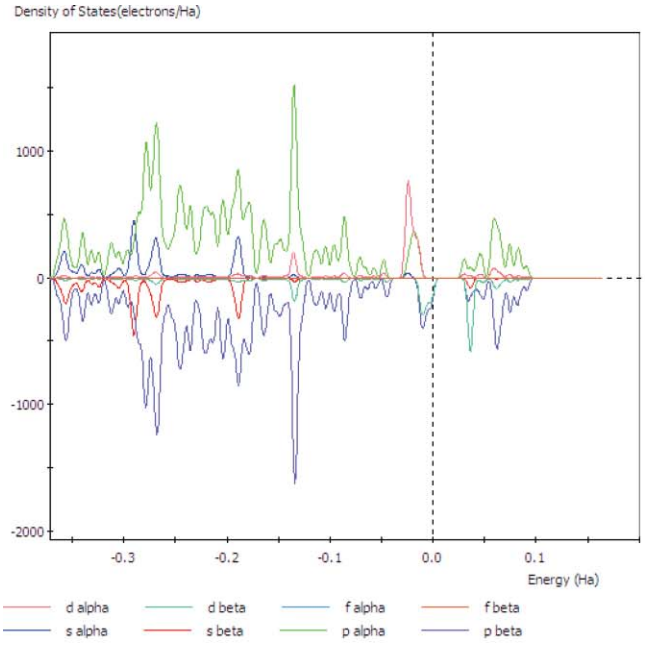

FIG. 7. (a). Spin resolved density of states in 4-VMB–Gr. (b) Spin resolved density of states in 4-FeMB–Gr.

IV. CONCLUSIONS

We have studied the electronic characteristics of MA-functionalized graphene and have shown that the metal-arene adducts mainly preserve the sp^2 hybridization network of the carbons on graphene away from the functionalizing groups. However, the π-conjugation of graphene near the Fermi level is greatly modified by the π-backbonding process, caused by d-orbitals of the metal atom in the functionalizing molecule, which leads to opening of a substantial bandgap dependent upon the adduct concentration and number of the occupied d-orbitals. Bandgaps vary from 0.81 eV for 4-CrBA–Gr to 0.11 eV for 1-VBA–Gr, and to zero for 1-FeBA–Gr and 4-MnBA–Gr. Moreover, the electronic structure of the functionalizing metal in the MA molecules allows the possibility of controlled modification of both the bandgap itself and the position of the Fermi level with respect to the "d-impurity" levels and native graphene bands. Some functionalizing molecules result in a ferromagnetic behavior along with the opening of the bandgap. Such dependence of the electronic properties on the type of functionalizing metal suggests a novel tunable approach for the "band engineering" of graphene. Our findings on the nature of MA-functionalization induced bandgap provide useful guidelines for enabling flexibility and optimization of graphene-based nanodevices.

ACKNOWLEDGMENTS

Sharp Laboratories of America is acknowledged for computational support. We also gratefully acknowledge the referees for their valuable remarks and suggestions during review of the manuscript.

[1]A. K. Geim and K. S. Novoselov, Nature Mater. **6**(3), 183 (2007); M. J. Allen, V. C. Tung, and R. B. Kaner, Chem. Rev. **110**, 132 (2010).
[2]C. Rao, A. Sood, K. Subrahmanyam, and A. Govindaraj, Angew. Chem., Int. Ed. **48**(42), 7752 (2009); A. Castro Neto, F. Guinea, N. M. R. Peres, K. S. Novoselov, and A. K. Geim, Rev. Mod. Phys. **81**, 109 (2009).
[3]V. M. Pereira, A. H. Castro Neto, and N. M. R. Peres, Phys. Rev. B **80**(4), 045401 (2009).
[4]B. Trauzettel, D. V. Bulaev, D. Loss, and G. Burkard, Nat. Phys. **3**, 192 (2007); K. Nakada, M. Fujita, G. Dresselhaus, and M. S. Dresselhaus, Phys. Rev. B **54**(24), 17954 (1996); L. Brey and H. A. Fertig, *ibid.* **73**(23), 235411 (2006).
[5]K. A. Ritter and J. W. Lyding, Nature Mater. **8**(3), 235 (2009).
[6]X. Li, X. Wang, L. Zhang, S. Lee, and H. Dai, Science **319**(5867), 1229 (2008).
[7]E. V. Castro, K. S. Novoselov, S. V. Morozov, N. M. R. Peres, J. M. B. L. dosSantos, J. Nilsson, F. Guinea, A. K. Geim, and A. H. CastroNeto, Phys. Rev. Lett. **99**(21), 216802 (2007); E. McCann, Phys. Rev. B **74**(16), 161403 (2006); Y. Zhang, T.-T. Tang, C. Girit, Z. Hao, M. C. Martin, A. Zettl, M. F. Crommie, Y. R. Shen, and F. Wang, Nature (London) **459**(7248), 820 (2009).
[8]K. F. Mak, C. H. Lui, J. Shan, and T. F. Heinz, Phys. Rev. Lett. **102**(25), 256405 (2009).
[9]D. K. Samarakoon and X.-Q. Wang, ACS Nano **4**, 4126 (2010).
[10]D. C. Elias, R. R. Nair, T. M. G. Mohiuddin, S. V. Morozov, P. Blake, M. P. Halsall, A. C. Ferrari, D. W. Boukhvalov, M. I. Katsnelson, A. K. Geim, and K. S. Novoselov, Science **323**(5914), 610 (2009); O. Leenaerts, B. Partoens, and F. M. Peeters, Phys. Rev. B **80**(24), 245422 (2009).
[11]M. Z. S. Flores, P. A. S. Autreto, S. B. Legoas, and D. S. Galvano, Nanotechnology **20**(46), 465704 (2009).
[12]J. Choi, K.-j. Kim, B. Kim, H. Lee, and S. Kim, J. Phys. Chem. C **113**(22), 9433 (2009); M. Quintana, K. Spyrou, M. Grzelczak, W. R. Browne, P. Rudolf, and M. Prato, ACS Nano **4**(6), 3527 (2010).
[13]L.-H. Liu and M. Yan, Nano Lett. **9**(9), 3375 (2009); L.-H. Liu, M. M. Lerner, and M. Yan, *ibid.* **10**(9), 3754 (2010).
[14]L.-H. Liu, G. Zorn, D. G. Castner, R. Solanki, M. M. Lerner, and M. Yan, J. Mater. Chem. **20**(24), 5041 (2010); L.-H. Liu, G. Nandamuri, R. Solanki, and M. Yan, J. Nanosci. Nanotechnol. **11**, 1288 (2011).
[15]A. V. Krasheninnikov, P. O. Lehtinen, A. S. Foster, P. Pyykko, and R. M. Nieminen, Phys. Rev. Lett. **102**(12), 126807 (2009).
[16]K. Suggs, D. Reuven, and X.-Q. Wang, J. Phys. Chem. C **115**(8), 3313 (2011).
[17]DMOL3, Accelrys Software Inc., San Diego, CA, 2010.

[18]A. D. Becke, Phys. Rev. A **38**(6), 3098 (1988); C. Lee, W. Yang, and R. G. Parr, Phys. Rev. B **37**(2), 785 (1988).
[19]S. H. Vosko, L. Wilk, and M. Nusair, Can. J. Phys. **58**(8), 1200 (1980).
[20]A. Ishii, M. Yamamoto, H. Asano, and K. Fujiwara, J. Phys.: Conf. Ser. **100**, 052087 (2008); K. Suggs, D. Reuven, and X.-Q. Wang, J. Phys. Chem. C **115**, 3313 (2011).
[21]V. Zólyomi, Á. Rusznyák, J. Koltai, J. Kürti, and C. J. Lambert, Phys. Status Solidi B **247**, 2930 (2010).
[22]O. Leenaerts, B. Partoens, and F. M. Peeters, Appl. Phys. Lett. **92**, 243125 (2008).
[23]R. L. Brandon, J. H. Osiecki, and A. Ottenberg, J. Org. Chem. **31**(4), 1214 (1966).
[24]C. N. R. Rao, K. S. Subrahmanyam, H. S. S. Ramakrishna Matte, B. Abdulhakeem, A. Govindaraj, B. Das, P. Kumar, A. Ghosh, and D. J. Late, Sci.Technol. Adv. Mater. **11**(5), 054502 (2010).
[25]D. Astruc, *Organometallic Chemistry and Catalysis* (Springer, Berlin, 2007), p. 251.
[26]C. Elschenbroich and R. Möckel, Angew. Chem. **89**(12), 908 (1977); E. P. Kundig and P. L. Timms, J. Chem. Soc., Chem. Commun. **1977**(24), 912.
[27]S. M.-M. Dubois, Z. Zanolli, X. Declerck, and J.-C. Charlier, Eur. Phys. J. B **72**, 1 (2009).
[28]A. D. McNaught and A. Wilkinson, *IUPAC: Compendium of Chemical Terminology* (*the "Gold Book"*), 2nd ed. (Blackwell Scientific Publications, Oxford, 2006).